BIOCYBERNETICS AND BIOMEDICAL ENGINEERING 41 (2021) 1561–1574

Available at www.sciencedirect.com

ScienceDirect

journal homepage: www.elsevier.com/locate/bbe

Original Research Article

A novel deep recurrent convolutional neural network for subthalamic nucleus localization using local field potential signals

Mohamed Hosny [a,c], *Minwei Zhu* [b], *Yixian Su* [a], *Wenpeng Gao* [a,*], *Yili Fu* [a]

[a] *School of Life Science and Technology, Harbin Institute of Technology, 2 Yikuang Str., Nangang District, Harbin 150080, China*

[b] *Department of Neurosurgery, First Affiliated Hospital of Harbin Medical University, 23 Youzheng Str., Nangang District, Harbin 150001, China*

[c] *Department of Electrical Engineering, Benha Faculty of Engineering, Benha University, Benha, Egypt*

ARTICLE INFO

Article history:
Received 16 July 2021
Received in revised form
30 August 2021
Accepted 26 September 2021
Available online 08 October 2021

Keywords:
Recurrent convolutional neural network
Deep learning
Subthalamic nucleus detection
Parkinson's disease
Deep brain stimulation
Local field potentials

ABSTRACT

Deep brain stimulation (DBS) of the subthalamic nucleus (STN) is a well-established interventional treatment for improving motor symptoms of patients suffering from Parkinson's disease (PD). While STN is originally localized using imaging modalities, additional intraoperative guidance such as microelectrode recording (MER) is crucial to refine the final electrode trajectory. Analysis of MER by an experienced neurophysiologist maintains good clinical outcomes, although the procedure requires long duration and jeopardizes the safety of the surgery. Lately, local field potentials (LFP) investigation has inspired the emergence of adaptive DBS and revealed beneficial perception of PD mechanisms. Several studies confronting LFP analysis to detect the anatomical borders of STN, have focused on handcrafted feature engineering, which does not certainly capture delicate differences in LFP. This study gauges the ability of deep learning to exhibit valuable insight into the electrophysiological neural rhythms of STN using LFP. A recurrent convolutional neural network (CNN) strategy is presented, where local features are extracted from LFP signals via CNN, followed by recurrent layers to aggregate the best features for classification. The proposed model outperformed the state-of-the-art techniques, yielding highest average accuracy of 96.79%. This is the first study on the analysis of LFP signals to localize STN using deep recurrent CNN. The developed model has the potential to extract high level biomarkers regarding STN region, which would boost the neurosurgeon's confidence in adjusting the trajectory intraoperatively for optimal lead implantation. LFP is a robust guidance tool and could be an alternative solution to the current scenario using MER.

* Corresponding author at: Building 2E, Science Park of Harbin Institute of Technology, Yikuang Str. 2, Nangang District, Harbin 150080, China.
E-mail address: wpgao@hit.edu.cn (W. Gao).

https://doi.org/10.1016/j.bbe.2021.09.005

1. Introduction

Parkinson's Disease (PD) is a chronic and quickly evolving long-term neurodegenerative disease. An estimated 10 million people succumbed to PD-related ailments[1]. At present, following Alzheimer's disease, PD is the second most prevalent neurodegenerative disorder [2], such as more than 150 000 PD patients are treated worldwide [3]. PD affects the basal ganglia (BG), owing to deficiency of dopamine [4], leading to major motor symptoms including bradykinesia [5] and tremor [6] as well as increasingly identified non-motor symptoms for instance, cognitive dysfunctions and sleep disorders [7]. Consequently, PD patients suffer from difficulty in movement initiation and control. Until now, primary causes are not well recognized yet, which several genetic, lifestyle and environmental factors. Due to the lack of full understanding of the neural mechanisms behind the PD disorder, there is no cure for PD, increasing the need for robust management of the disease to alleviate the main symptoms whether pharmacotherapy [8] or interventional [9].

Deep brain stimulation (DBS) of the three frequently chosen targets, namely, bilateral ventral intermediate nucleus (VIM) of the thalamus, subthalamic nucleus (STN) [10] and medial globus pallidus (mGP) [3], is currently the most dominant and potent surgical treatment for advanced PD patients to control dopamine-related motor symptoms in cases where they are no longer reactive to pharmacological approaches [11]. DBS is accomplished by implanting permanent electrodes in the brain which deliver continuous high-frequency stimulation to the designated target regions. However, similar to most intracranial neurosurgical procedures, achieving great therapeutic outcomes and success of the interventional procedure can be significantly decided by the optimal positioning of the stimulating DBS lead in the target structure [12,13]. Besides, sub-optimal placing of DBS electrodes provokes up to 48.5% of revisions in interventional neurostimulation treatments [14].

During the preoperative surgical planning stage, the relevant craniotomy position on the skull, the optimal target coordinates in the stereotactic frame space and the corresponding electrode insertion trajectories are identified based on the fusion of magnetic resonance (MR) imaging and intraoperative stereotactic computer tomography (CT) sequences as a typical procedure of the clinical care. In addition to the anatomical information, other preoperative imaging modalities (e.g. functional MR and positron emission tomography (PET)) could be employed to extract the functional characteristics of the STN structure in order to determine the trajectory depth and the stereotactic angles [15]. Nevertheless, using neuroimaging alone as the guiding modality does not assure precise locating of the DBS electrode in the defined target during the operation. These imaging modalities can just provide the approximate position of the target, because of several reasons, for instance, resolution limitations of images and possible distortion as well as potential mechanical errors in stereotactic frame space registration [2]. Besides, displacing of the identified target coordinates due to additional deformations derived from anatomic shifts with the craniotomy. Moreover, authors in [16] reported that exploiting MR imaging solely in intraoperative STN detection would cause up to 20% of cases with sub-optimal electrode insertion.

Thus, an additional real time fine-tuning to the electrode trajectory via intraoperative modality is crucial to mitigate the aforementioned encumbrances, account for sources of potential errors and guarantee accurate implantation. This fine-tuning would help to expose the underlying neuroanatomical structures of interest and pinpoint the final localization of the STN. PD patients are commonly awake during the surgery (i.e. patient is under only local anesthesia which preserves the wakefulness), this allows for real time corrections to be made in the electrodes positioning based on the immediate motor symptoms response to a small amount of test stimulation [17]. In contrast, this process is used to imply the optimal alignment of the target with respect to the clinical effects of the applied stimulation on the patient's symptomatology (i.e. motor disorder control and induced side effects). As a result, additional motor activities are incorporated for guidance and the best place to apply stimulation is not delineated purely anatomically but also functionally. Despite that this method is demanded, it necessitates the patient to be in conscious state and performs extra movements, thus, adds a source of discomfort to the procedure. Also, this could threaten the safety of the surgery, in particular, patients with severe motor symptoms. Furthermore, this method would be complicated in case the number of trial-and-error attempts increases. Moreover, it is not always possible for different anesthesia techniques, especially global anesthesia where the patient is not awake and therefore, the available information to the surgical team is limited and the success rate is lower. Accordingly, another adjunctive source of information from intraoperative guidance is critical regardless of the type of anesthesia employed [18].

Currently, interventional MR (iMR) imaging is a possible solution and has proved to be successful in confirming or refining the anatomical placement of the electrode during the DBS surgery. However, this method entails a specially designed MR room which would be significantly expensive [19]. Microelectrode recording (MER) which maintains good clinical outcomes as with iMR imaging, is an alternative tool for final trajectory refinement [20]. Often, MER is employed intraoperatively to capture the electrophysiological activity of neurons close to the electrode tip at defined intervals along the trajectory. The neurophysiological characteristics of the targeted structure (inside STN) is divergent from other structures in the surrounding areas (outside STN) in terms of spike background activity and firing rate. Also, STN is associated with higher density of neurons and background noise in addition to the presence of large peaks corresponding to spontaneous discharge activity [21]. Therefore, as the recorded MER reflects the neural population in the closest vicinity of the electrodes, a trained neurophysiologist or highly experienced neurosurgeon can visualize and/or listen to MER signals with the goal of localizing the anatomical boundaries of STN.

While MER is effective in its use and offers significant information of the electrophysiological pattern inside STN which are important for neuronavigation, the procedure jeop-

ardizes the safety of the surgery and suffers from several limitations. Such as employing multiple electrodes with sharp tips which could lead to intracranial hemorrhage within the microelectrode trajectory [22,23]. Besides, the complexity of mental interpretation of MER signal patterns [24] and the susceptibility to several types of artifacts[21]. Also, the mislabeling of STN borders owing to similar spiking characteristics or uninterrupted transition from STN to substantia nigra (SNR) [25]. Moreover, the subjective judgment to affirm each recording increases the surgery time and opens the door for human error.

All the challenges discussed above justify the interest in further considering a more robust guidance tool for accurate implantation of the DBS electrode with the patient in an unconscious state in order to reduce the surgery time, ameliorate the patient comfort and improve the safety of the procedure. Local field potentials (LFP) which render the aggregate activity of neuronal populations within a larger diameter from the electrode contact, have been regarded as a significant indicator of electrophysiological neural rhythms for detection of STN region in PD [26–29]. Fig. 1 and Fig. 2 display unique typical bispectrum plots of STN and non-STN LFP signals. It is clear that the bifrequency magnitude is distinguishing for each class. Also, most of the magnitude of the bispectrum lies within −0.02 to 0.02 and there is a random distribution of the magnitudes at various frequencies.

Overall, MER as well as LFP have valuable potential to reveal hidden footprints of PD disorder. Nevertheless, the examination of these signals is a tiresome job even for an expert neurosurgeon. Hence, proposing a computer-aided STN detection system helps neurosurgeons in supporting the decline STN localization errors and obtaining a significant opinion about the optimal electrode trajectory during the surgery. Up to now, most of the developed approaches for automatic detection of STN borders have focused on MER analysis [2,12,24,30,31]. However, other studies were carried out to correlate LFP features with automated localization of the STN region [22,23,32,33]. In [22], Telkes et al. investigated the frequency profile of the LFP signals via exploring the frequency-depth analysis in accordance with the time–frequency analysis. Then, normalized energy features calculated

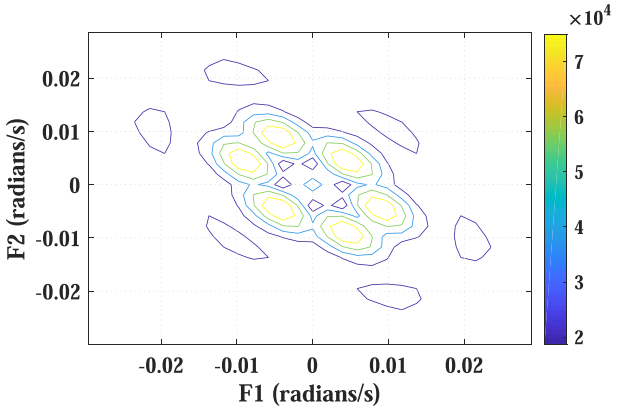

Fig. 1 – Bispectrum plot of the average of 1000 randomly chosen LFP samples from STN region.

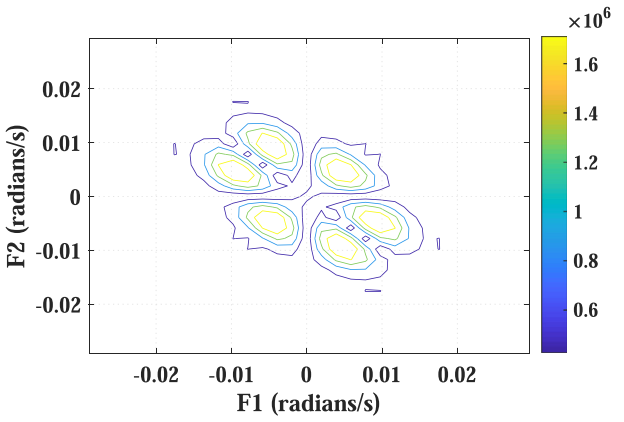

Fig. 2 – Bispectrum plot of the average of 1000 randomly chosen LFP samples from Non-STN region.

from the spectrum of different sub-bands were employed to identify the neurophysiological borders of STN. Their experiments demonstrated that the frequency content of beta and gamma bands are strongly representative of the dorsal STN border presence, while the other bands did not provide distinguishing characteristics. They reported that LFP could be a possible alternative solution to MER for targeting STN during DBS surgery. In this regard, Cao et al. [33] inferred that power band ratios of LFP signals in the frequency ranges (16–20 Hz), (20–30 Hz) and (100–250 Hz) present vital signatures for detection of functional regions in the BG area. These results are consistent with previous studies on the automated identification of STN using MER signals. Such as, Valsky et al. [25] verified that 100–150/5–25 Hz power ratio furnishes a reliable discrimination between STN and SNR, and yielded an accuracy of 94%. Similarly, Cagnan et al. [34] revealed that background neural activity and spectral features of beta (13–30 Hz) and gamma (31–100 Hz) bands show different values inside STN compared with outside STN. As reported therein, their method achieved an accuracy of 88%. Also, LFP signals acquired from STN sub-territories manifest discriminating neurophysiological characteristics concerning the motor sub-types of PD [27]. While authors in [26] explored the spectral features extracted from directional LFP signals with the goal of finding markers to select the optimal contacts.

It is evident that several models have been implemented to support STN identification based on Machine Learning (ML) strategies. These traditional ML techniques hinge on handcrafted feature extraction from different neurophysiological signals, LFP, which are eventually classified by different algorithms either supervised [32] or unsupervised [28]. Meanwhile, advances in terms of available computing power and algorithms have exhibited the use of deep learning (DL) methods typically, convolutional neural network (CNN) and recurrent neural network (RNN), in automated detection of STN are on the increase. MER signals classification in the context of STN detection using DL algorithms to ameliorate the performance has similarly been on the rise. Khosravi et al. [30] proposed an early design of a deep neural network (DNN) binary classifier to identify the borders of STN. They demonstrated the ability of wavelet transform (WT) to display

the frequency profile of MER signals and extract distinguishing features. Using artificial neural network (ANN), they yielded highest classification accuracy of 92%. In parallel, in 2021, the work of Martin et al. [2] has led to the development of dynamic DL approaches to deal with the complexity of MER signals, reporting that a Bayesian extension using features obtained from 1D CNN achieved the highest performance with accuracy of 83.5%. However, to our best knowledge no studies have pursued to quantify and localize the STN region using DL concept based on LFP signals. Herein, a new effective 19-layered recurrent convolutional network is developed to identify the dorsal and ventral borders of STN. The primary goal of our study emphasizes on divulging the importance of intraoperative LFP neural signals and clarifying their predictive role in terms of STN localization during DBS surgery. A DL approach is implemented in order to personalize the evidence-based DBS implantation procedure and validated it using 17 PD patients. Moreover, this model is able to reveal the neural basis from LFP signals without the focus on typical design of feature extraction or selection and classification protocols as enumerated earlier in previous studies. This circumvents the inherent shortcomings corresponding to training ML models, especially on big data of LFP recordings. As the implemented recurrent CNN model is capable of aggregating the best fusion of feature extraction and classification.

Furthermore, three longstanding feature extraction techniques are utilized in this study. Then, the performance of the developed model is evaluated alongside the three feature groups. The comparison in the manner mentioned above is crucial to confront the performance of the proposed model against the traditional methods in the area of LFP analysis. First power band and peak-to-average power ratios of the LFP signals in different frequency sub-bands (i.e. delta, theta, alpha, low beta, middle beta, high beta, gamma and high gamma) were extracted as in [28,35]. Second statistical moment features of the Hilbert-Huang marginal spectrum (HMS) of the same aforementioned frequency sub-bands were extracted based on previous studies [28,36]. Third we developed wavelet packet transform (WPT) based features similar to the reported in [24] as a reliable source of information for distinguishing between MER signals stem from inside and outside STN. Consequently, each feature group was classified using 10 conventional ML classifiers. From the results of the presented comparison, it can be inferred that the proposed recurrent CNN model betters the other methods in terms of accuracy for the dataset employed.

2. Methods

2.1. Data acquisition and preprocessing

The dataset analyzed in this study includes LFP signals of 32 trajectories collected from 17 idiopathic PD patients (10 males and 7 females; age: 62.2 ± 5.7 years) undergoing a routine single or bilateral insertion during DBS surgery at the First Affiliated Hospital of Harbin Medical University, Harbin, China. The mean disease duration was 10 ± 3.5 years. All patients were inserted in STN using one microelectrode. LFP recordings were obtained from 10.0 mm to −4.0 mm with respect to the predetermined target. Commonly, the electrode advance was fixed in 1.0 mm and 0.5 mm steps at depth from 10 mm to 5 mm and from 5 mm to 4 mm below the estimated surgical zero-point, in that order. In parallel to the data acquisition, LFP recordings were annotated as either inside STN (STN) or outside STN (Non-STN) by an expert neurosurgeon. LFP recordings were acquired with the NeuroNav system (Alpha Omega Engineering, Israel), which also measures the LFP distance from the estimated target. Each recording was sampled at 760 Hz after being digitally filtered with 50 Hz notch filter. All study subjects had provided informed consent. LFP signals were segmented into 1-s segments. Thus, the dataset contains a total of 4248 1-s LFP signals, where 2627 signals are labeled as being inside the STN and the remaining 1621 signals are labeled as outside the STN. LFP dataset used in this work is illustrated in Table 1.

2.2. Data scaling

After segmentation, normalization technique is applied. To normalize our dataset, Min–max method is utilized to transform each LFP recording consisting of 760 sampling points into the common range [0,1] for further analysis. The normalization approach employed here is patient-independent such as the minimum and maximum parameters are calculated from the entire LFP recordings. In this work, normalization procedure is important to get rid of the amplitude scaling problem, group the data together in a small range of values and handle the bias to larger values before being fed to the developed DL model for training and testing.

2.3. Feature extraction from LFP

In this work, in the first feature group, we extracted the power band ratios (i.e. power of the signal in a certain band divided by the total power) and peak-to-average power ratios of the LFP signals in the following frequency sub-bands, delta (0.1–3 Hz), theta (4–7 Hz), alpha (8–12 Hz), low beta (12–16 Hz), middle beta (16–20 Hz), high beta (20–30 Hz), gamma (30–100 Hz) and high gamma (100–250 Hz). In the second feature group, for each sub-band (i.e. the aforementioned frequency sub-bands), first empirical mode decomposition was employed to extract the intrinsic mode functions (IMF) which include the significant frequencies of interest of the LFP signal. Then, HMS which represents the time-energy-frequency distribution, was obtained by applying Hilbert-Huang transform to each IMF. After that, seven statistical moments namely, max-

Table 1 – Description of the collected LFP dataset.

Patients	Trajectories	Sampling frequency	STN (s)	Non-STN (s)	Total (s)
17	32	760	2627	1621	4248

imum, variance, energy, Shannon's entropy, mean value, Skewness and Kurtosis, were calculated from HMS. In the third feature group, we decomposed the LFP signals using WPT with Daubechies 4 into five levels. Then, for each sub-band (i.e. 32 sub-bands), two statistical parameters namely, standard deviation and energy were calculated. To sum up, we extracted three feature groups where the first group includes 16 features (8 power band ratios and 8 peak-to-average power ratios), the second group includes 56 HMS based features and the last group contains 64 WPT based features. In the subsequent sections, we will denote the first, second and third feature groups as Power, HHT and WPD, respectively.

Ten ML classifiers were employed to evaluate the performance of the features discussed earlier. Decision tree (Tree), five Boosting algorithms (AdaBoostM1, Bagging, GentleBoost, LogitBoost and RobustBoost), k-Nearest Neighbour (KNN) and support vector machine (SVM) with radial basis function (RBF), polynomial (Poly) and linear kernels were utilized.

2.4. *Proposed deep learning model*

A DL model is implemented herein to achieve good classification performance on LFP signals in order to detect the STN region. DL is another type of artificial neural networks established with mathematical manipulation which has the ability to convert an input state into an output by various layers processing of the input and unit-wise computation of the probability of each output [21]. Higher computational complexity emerges from increasing the number of deep layers where each neural network layer performs the mathematical manipulation. The morphology of the LFP waveform declares the required features for classification, therefore handcrafted feature extraction algorithms are critical to characterize LFP signals via group of parameters. Convolution layers in CNN have been proven efficient in exposing the hidden non-linear features from raw data which manifests good signal to noise ratio [37]. However, it is neither potent nor convenient to depend solely on CNN, because morphological features of LFP signals can be difficult to categorize and very complex due to the fact that the duration of these recordings could extend to ten seconds. Also, the possible presence of irrelevant or redundant parts. In view of this, CNN model is designed for local feature extraction from the LFP signals and RNN layers such as long short-term memory (LSTM) or Gated Recurrent Unit (GRU) are utilized to summarize the local feature series. Consequently, the proposed recurrent CNN model comprises of three parts: namely, local feature extraction (LFE), global feature extraction (GFE) and classification. The proposed model fuses LFE and GFE parts to produce a prodigious yet efficient system for the detection of STN boundaries. Accomplishment of the proposed system requires feeding the segmented normalized LFP signals (1-s) into the CNN model where optimum combination of deep features are extracted. Following that, recurrent layers are used to transform the deep feature maps into global vectors ready for classification. Dense layers are employed to retain the deep feature maps and categorize them into different classes following which final location is identified, i.e., STN or Non-STN. Fig. 3 presents the detailed architecture of the proposed recurrent CNN model as stated earlier. Table 2 illustrates each layer in the proposed model. The remainder of this subsection explains details of the three parts that formulate the proposed model.

2.4.1. *Local feature extraction (LFE)*

LFE part has been optimized to compose uncomplicated layers, that focused on raw LFP signals to exhibit the morphological characteristics of 1-s LFP recording and produce a sequence of local features. CNN is used to construct the LFE part as discussed earlier. As shown in Fig. 3, normalized LFP signals are fed to the input layer. Then, a series of repeating structures (i.e. Each structure is made up of convolution, batch normalization and pooling layers) are applied hierarchically on the input signals. Convolution layers are used to extract substantial feature maps with different sizes. The kernel size of the first Convolution layer in the first structure is assigned at 9, decreased by 2 for the second structure, then through every 2 structures, the kernel size is decreased by 2. Batch normalization layer is inserted after the convolution layer to set the LFP signals into a certain range of values so as to accelerate the learning process. Therefore, faster convergence is guaranteed during training. Max pooling layers whose size is 2 are employed to progressively decrease the dimensionality of the feature maps via keeping only the highest numbers in every kernel which characterize the most pivotal features. As a result, the number of parameters is reduced, which helps to manage the computational complexity and overfitting problem. The LFE part ends with an average pooling layer, then the feature maps are injected to the GFE part.

2.4.2. *Global feature extraction (GFE)*

In GFE part, the feature maps are converted into global vectors. Two recurrent layers with 128 and 64 neurons are employed to specify the characteristics of the global vectors that emanate from the last layer of each recurrent network. The number of hidden units in the recurrent layer determines the vector length. Therefore, GFE decides which features to keep from the LFE part at each time step, before feeding them to the classification part. LSTM and GRU were tested as the recurrent layer. The number of trainable parameters in the slightly more complex LSTM layers is higher than GRU layers (i.e. see Table 2).

2.4.3. *Classification*

Classification is the last part of the proposed recurrent CNN model. Two dense layers are used to learn the feature vectors and classify the input LFP signal into two classes based on the predicted probabilities, i.e., STN or Non-STN. The first dense layer is followed by a rectified linear unit (ReLU), where the last dense layer has one cell and followed by the final activation layer SoftMax, which produces the probability of each class.

2.4.4. *Implementation details*

Grid search technique was employed to optimize all the hyperparameters including kernel size, number of CNN filters, neurons in the dense layer and number of recurrent memory units. The training mini batch size was set as 128.

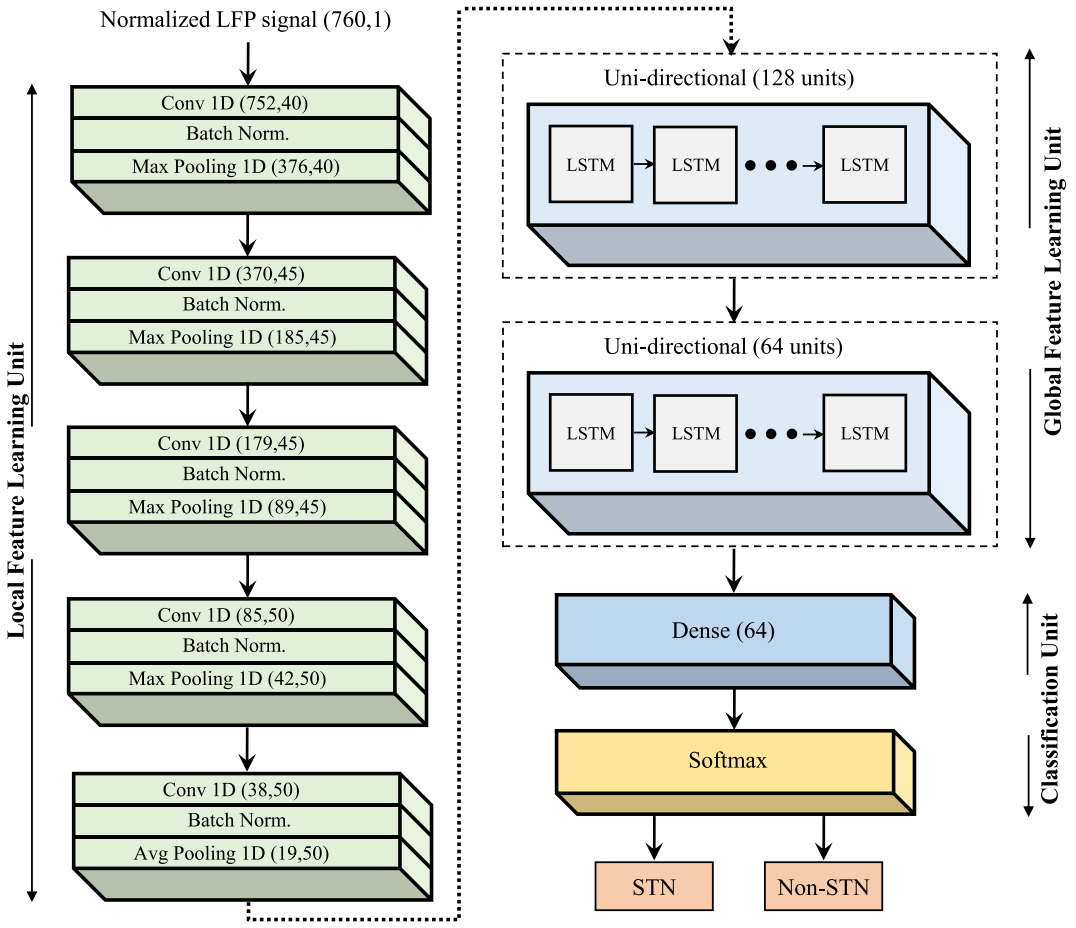

Fig. 3 – Architecture of the proposed DL model using LSTM as the recurrent layer.

Table 2 – Specifics of each layer in the proposed recurrent CNN architecture.

No.	Layer name	Kernel size	No. of filters	Layer Params.	Output shape	Number of Params.
0	Input	-	-	-	760 × 1	0
1	Conv 1D	9 × 1	40	Stride = 1, Activation = ReLU	752 × 40	400
2	Batch Norm.	-	40	-	752 × 40	160
3	Max Pooling 1D	2 × 1	40	Stride = 2	376 × 40	0
4	Conv 1D	7 × 1	45	Stride = 1, Activation = ReLU	370 × 45	12645
5	Batch Norm.	-	45	-	370 × 45	180
6	Max Pooling 1D	2 × 1	45	Stride = 2	185 × 45	0
7	Conv 1D	7 × 1	45	Stride = 1, Activation = ReLU	179 × 45	14220
8	Batch Norm.	-	45	-	179 × 45	180
9	Max Pooling 1D	2 × 1	45	Stride = 2	89 × 45	0
10	Conv 1D	5 × 1	50	Stride = 1, Activation = ReLU	85 × 50	11300
11	Batch Norm.	-	50	-	85 × 50	200
12	Max Pooling 1D	2 × 1	50	Stride = 2	42 × 50	0
13	Conv 1D	5 × 1	50	Stride = 1, Activation = ReLU	38 × 50	12550
14	Batch Norm.	-	50	-	38 × 50	200
15	Avg Pooling 1D	2 × 1	50	Stride = 2	19 × 50	0
16	LSTM/GRU	-	-	128 units, sequence-to-sequence	128	552448/414720
17	LSTM/GRU	-	-	64 units, sequence-to-label	64	49408/37248
18	Dense	-	-	Activation = ReLU	64	4160
19	Softmax	-	-	Activation = Softmax	2	130

Norm. = Normalization, Params. = Parameters.

Adam stochastic optimizer with learning rate of 0.001 was used for training using the backpropagation algorithm. Binary cross-entropy was employed as the loss function and accuracy was computed to determine the convergence. Overfitting is a huge concern during local feature learning process. To ameliorate the generalization, only 40 epochs were selected for training the network. The developed models are implemented on MATLAB (MATLAB and Neural Network Toolbox Release 2021a, The MathWorks, Inc., Natick, Massachusetts, United States). The hardware environment in this study is a computer with an Intel Core i5-8400 CPU, a Nvidia GeForce GTX 1060 GPU and 16 GB memory.

2.5. *Performance evaluation and metrics*

To elude any ascendancy associated with biasing and data leakage, leave-one-patient-out-cross-validation (Leave CV) was used to assess the performance of the implemented networks and the ML classifiers on a database of 4248 1-s LFP samples obtained from 17 patients with PD. Therefore, eventually there were 17-fold cross-validation iterations. For each fold, the same model was employed and the training dataset was constructed from LFP samples originate from 16 patients, while the testing dataset was constructed from LFP samples drawn from the left patient. This process was repeated for 17 times. The average over the 17 folds was calculated to estimate the final performance. By doing this, we ensured that LFP samples from the same patient will not appear in both training and testing datasets and more importantly each method is trained and tested on the same datasets to verify the comparative study. To further gauge the efficacy of the proposed methods, five frequently used metrics, i.e., accuracy (Acc), sensitivity (Sens), specificity (Spec), F1-score and precision, were employed to evaluate the classification performance. The latter two measure criteria are less influenced by data imbalance. The mathematical formulation of the five metrics are defined below:

$$Acc = \frac{TP + TN}{TP + TN + FP + FN} \tag{1}$$

$$Sens = \frac{TP}{TP + FN} \tag{2}$$

$$Spec = \frac{TN}{TN + FP} \tag{3}$$

$$Precision = \frac{TP}{TP + FP} \tag{4}$$

$$F1 - score = \frac{(2 \times Sens \times Pre)}{Sens + Pre} \tag{5}$$

Where TP, TN, FP and FN are the true positive, true negative, false positive and false negative rates of classification, in that order.

3. Results

In this section, the performance of the proposed methods are presented and validated on 4248 1-s LFP signals from 17 PD patients. Specifically, the proposed two recurrent CNN models are validated via three feature extraction techniques (i.e. see Section 2.3). Therefore, three feature groups (HHT, Power and WPD) were extracted, followed by 10 ML classifiers for classification. As mentioned, the developed CNN network was embedded with two recurrent layers (LSTM and GRU) to produce two end-to-end models, LSTM CNN and GRU CNN. Comparative experiments were held to compare between the three feature groups as well as to compare the performance of the proposed methods with the ML classifiers on LFP signals for STN region detection.

Fig. 4 illustrates the variations of statistical parameters namely, standard deviation and energy of three representative wavelet packet scales with corresponding frequencies of (0–11.875 Hz), (11.875–23.75 Hz) and (118.75–130.625 Hz) in the regions of STN and Non-STN. It can be seen that, the standard deviation of the wavelet packet coefficients in (0–11.875 Hz) is higher in STN region than Non-STN region (STN median: 0.11068, Non-STN median: 0.06424). Similarly, the energy of the coefficients is higher in the clinically estimated region of STN than the region of Non-STN. However, for the other two wavelet packet scales, an increasing trend can be seen in the median values of the statistical parameters of the wavelet packet coefficients in Non-STN region compared to STN region. The standard deviation of the wavelet packet coefficients in (11.875–23.75 Hz) is higher in Non-STN region than STN region (STN median: 0.01657, Non-STN median: 0.01858). The distributions of STN and Non-STN are similar for the energy of wavelet packet coefficients, as it is higher in the region of Non-STN than the region of STN. The standard deviation of the coefficients in (118.75–130.625 Hz) is higher in the region of Non-STN than the region of STN (STN median: 0.00303, Non-STN median: 0.00340).The energy of the coefficients is also found to have similar pattern of standard deviation. It is clear that WPD could maintain significant signatures for localizing the STN. Ten ML classifiers were utilized to gauge the applicability of WPD in comparison with two existing features. The average and standard deviation of performance metrics of the ML classifiers with the three feature groups in the classification problem, Non-STN vs. STN, are presented in Table 3. Also, Fig. 5 and Fig. 6 display precision and F1-score performances of all ML classifiers for separating LFP signals into two classes using the three feature groups. Overall, WPD outperformed HHT and Power. HHT obtained higher results compared to Power.

Using WPD, it is found that GentleBoost performed better than the other ML classifiers. It yielded an average Acc of 92.64%, Sens of 91.79%, Spec of 94.52%, precision of 96.81% and F1-score of 93.54%. Therefore, among the boosting classifiers, GentleBoost achieved the highest performance, followed by AdaBoostM1 with 92.56% Acc. Between the SVM kernels, Poly2 obtained the highest Acc of 92.04%, which signify that the LFP signals are non-linear in nature. Likewise, in the case of using HHT, LogitBoost achieved higher performance than other classifiers. It obtained an average Acc of 86.08%, Sens of 85.80%, Spec of 86.56%, precision of 91.81% and F1-score of 87.69%. Similarly, the experimental results show that LogitBoost classifier achieved the highest performance with Power. It yielded an average Acc of 84.61%, Sens of 85.16%, Spec of 82.38%, precision of 89.73% and F1-score of 86.10%. Between the different SVM kernels, RBF attained the highest Acc of 77.06%

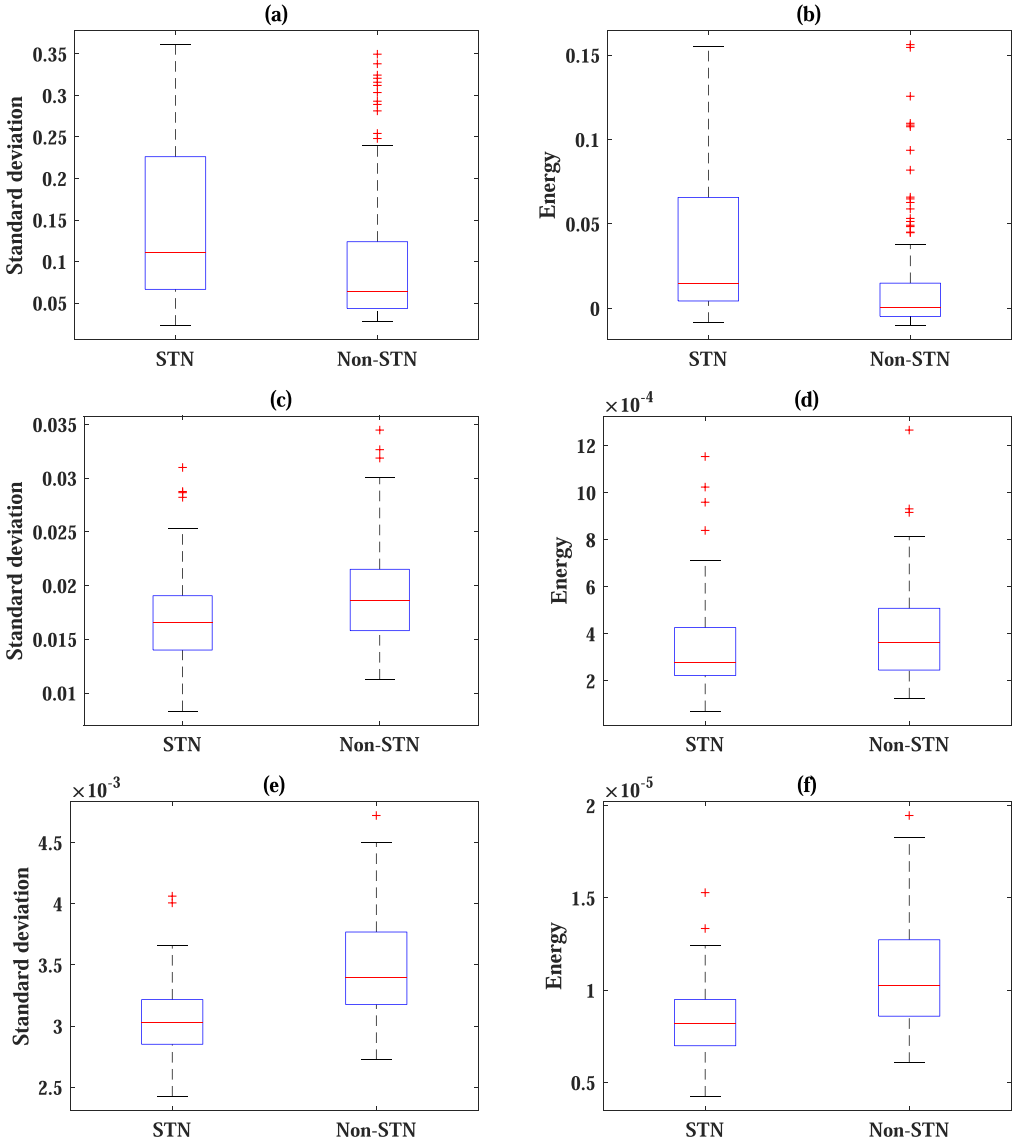

Fig. 4 – Standard deviation and energy of three wavelet packet coefficients in STN and Non-STN regions: (a), (b) for (0–11.875 Hz), (c), (d) for (11.875–23.75 Hz) and (e), (f) for (118.75–130.625 Hz). The box plots indicate the minimum and the maximum values. Boxes start from the 25th percentile and end at the 75th percentile. Red lines inside the boxes specify the median values.

The performance results of the proposed DL models are reported in Table 4. It is clear that the proposed recurrent CNN models outperformed the classical ML classifiers. LSTM CNN achieved the highest mean Acc of 96.79%, Sens of 97.91%, Spec of 93.68%, precision of 97.23% and F1-score of 97.48%, while GRU CNN obtained mean Acc of 96.59%, Sens of 96.80%, Spec of 95.47%, precision of 97.76% and F1-score of 97.01%. Performance measures encompassing Sens and Spec, which denote that the developed model can actually differentiate between STN and Non-STN classes, are especially pertinent. Therefore, Fig. 7 shows the plot of different measure criteria of the proposed LSTM CNN and GRU CNN alongside all ML classifiers with WPD. For STN class, LSTM CNN was able to accurately classify 97.91% of the LFP signals stem from the STN region. On the other hand, for Non-STN class, GRU CNN was able to accurately classify 95.47% of the LFP signals originate from the Non-STN region. Fig. 8 displays box plot of the Acc of ML classifiers with WPD as well as the proposed recurrent CNN models. These results suggest that the recurrent CNN models are efficient for all patients. The average training time of each epoch for LSTM CNN and GRU CNN is 4.566 and 4.524 s, in that order. While the average testing procedure for all the LFP signals of a patient has a roughly estimated time cost of 200 and 201 ms. The estimated time can be further decreased by fully optimized codes, high-end computers and GPUs. Moreover, usage of a language embedded in the working system, will dramatically reduce the computational time.

Table 3 – Mean values (± standard deviation) of classification measures of WPD in comparison to HHT and power. The validation is implemented using leave-one-patient-out strategy. Mean characterizes the average value of 17 patients.

Features	Classifier	Acc (%)	Sens (%)	Spec (%)	Precision	F1-score
HHT	Tree	85.13 ± 9.26	85.19 ± 14.31	85.71 ± 12.11	90.86 ± 8.11	87.05 ± 9.29
	AdaBoostM1	85.98 ± 9.34	85.90 ± 14.88	85.70 ± 13.25	91.44 ± 7.75	87.65 ± 9.66
	LogitBoost	86.08 ± 9.34	85.80 ± 15.33	86.56 ± 12.98	91.81 ± 7.60	87.69 ± 9.70
	Bagging	84.23 ± 10.05	83.40 ± 17.51	85.48 ± 15.57	91.11 ± 8.52	85.75 ± 11.02
	GentleBoost	85.85 ± 9.27	85.99 ± 15.24	85.75 ± 13.47	91.43 ± 7.78	87.58 ± 9.56
	RobustBoost	85.09 ± 9.34	85.47 ± 14.67	84.19 ± 12.95	90.21 ± 8.49	86.90 ± 9.82
	KNN	70.42 ± 17.15	95.39 ± 3.12	29.68 ± 40.52	71.63 ± 17.98	80.63 ± 11.52
	SVM RBF	71.05 ± 18.26	98.80 ± 1.53	25.36 ± 48.31	71.29 ± 18.54	81.59 ± 12.15
	SVM Poly2	69.47 ± 16.29	86.36 ± 22.68	44.25 ± 29.44	73.18 ± 13.24	76.11 ± 18.23
	SVM Linear	71.14 ± 18.45	99.68 ± 0.69	24.18 ± 50.85	71.07 ± 18.38	81.77 ± 12.23
Power	Tree	83.80 ± 8.53	85.62 ± 14.04	78.14 ± 20.60	88.15 ± 9.59	85.96 ± 9.61
	AdaBoostM1	84.14 ± 9.96	85.01 ± 16.64	81.72 ± 16.91	89.00 ± 9.89	85.74 ± 11.62
	LogitBoost	84.61 ± 10.05	85.16 ± 16.95	82.38 ± 17.81	89.73 ± 9.63	86.10 ± 11.75
	Bagging	81.68 ± 10.64	84.65 ± 16.41	76.57 ± 19.53	86.67 ± 11.43	84.29 ± 11.12
	GentleBoost	84.15 ± 9.91	85.05 ± 16.91	81.85 ± 16.44	89.27 ± 10.14	85.78 ± 11.55
	RobustBoost	82.88 ± 11.03	84.64 ± 17.53	79.43 ± 15.58	87.27 ± 10.94	84.68 ± 12.80
	KNN	75.34 ± 13.82	87.52 ± 12.13	55.47 ± 31.44	78.05 ± 16.18	81.33 ± 11.53
	SVM RBF	77.06 ± 12.73	84.95 ± 13.76	63.79 ± 30.23	81.06 ± 15.59	81.68 ± 11.38
	SVM Poly2	76.33 ± 10.04	83.23 ± 14.47	64.79 ± 24.84	81.09 ± 13.52	80.76 ± 9.78
	SVM Linear	75.34 ± 13.85	90.48 ± 11.88	49.64 ± 35.03	77.08 ± 16.47	81.89 ± 11.21
WPD	Tree	89.13 ± 8.65	91.15 ± 11.69	86.12 ± 16.99	91.72 ± 8.63	90.78 ± 8.23
	AdaBoostM1	92.56 ± 9.05	91.58 ± 13.60	94.63 ± 10.35	96.98 ± 5.23	93.50 ± 8.55
	LogitBoost	92.11 ± 8.98	91.47 ± 13.66	93.78 ± 11.81	96.40 ± 6.20	93.09 ± 8.53
	Bagging	90.26 ± 9.6738	88.22 ± 15.46	94.38 ± 8.90	96.47 ± 4.80	91.22 ± 9.60
	GentleBoost	92.64 ± 8.67	91.79 ± 13.33	94.52 ± 10.03	96.81 ± 5.17	93.54 ± 8.35
	RobustBoost	90.29 ± 9.82	90.49 ± 13.80	90.89 ± 14.63	94.69 ± 7.44	91.69 ± 8.85
	KNN	89.23 ± 9.28	91.32 ± 12.97	85.97 ± 15.06	91.92 ± 8.51	90.85 ± 8.90
	SVM RBF	91.49 ± 7.86	92.29 ± 12.15	87.21 ± 23.65	94.57 ± 6.61	92.73 ± 7.79
	SVM Poly2	92.04 ± 6.71	94.93 ± 4.32	86.09 ± 17.26	92.94 ± 7.64	93.77 ± 5.07
	SVM Linear	85.96 ± 18.99	87.15 ± 25.02	86.29 ± 19.02	92.41 ± 8.92	86.21 ± 23.46

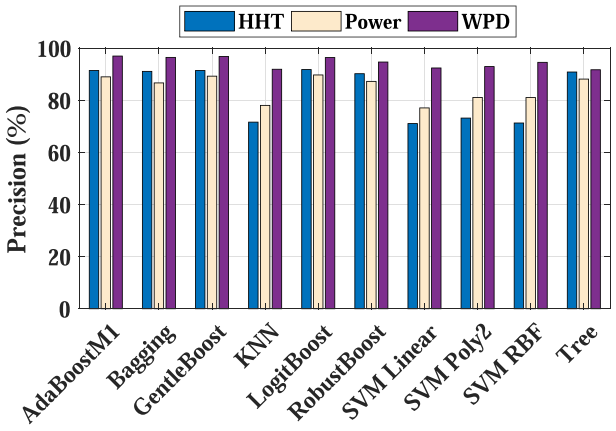

Fig. 5 – The bar plot of performance comparison of each classifier using the three feature groups in terms of precision.

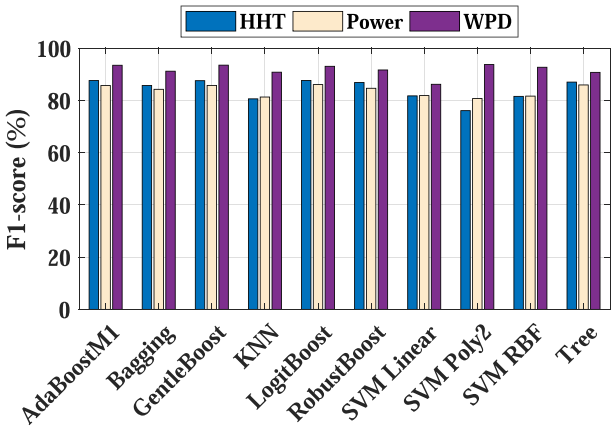

Fig. 6 – The bar plot of performance comparison of each classifier using the three feature groups in terms of F1-score.

4. Discussion

Stereotactic electrode implantation accuracy is a key component of DBS surgery, to obtain highest therapeutic benefit and evade counter complexities from stimulation. Imaging modalities have cited prominent patient comfort and very likely few brain insertions. Despite the advancements in these modalities [38], they possess inherent limitations, cannot relieve the underlying structures of interest and pinpoint the final target inside the STN region alone [39]. Therefore, additional intraoperative fine-tuning tool in surgeon's armamentarium to confirm the final electrode trajectory as a preoperative plan is pivotal. MER has been significantly proved to be a tool to discriminate between the sub-cortical struc-

Table 4 – Mean values (± standard deviation) of classification measures of DL classifiers using STN and Non-STN LFP signals based on leave-one-patient-out strategy.

Classifier	Acc	Sens	Spec	Precision	F1-score
LSTM CNN	96.79 ± 6.15	97.91 ± 5.48	93.68 ± 14.46	97.23 ± 5.87	97.48 ± 5.04
GRU CNN	96.59 ± 7.15	96.80 ± 9.56	95.47 ± 11.84	97.76 ± 5.30	97.01 ± 6.92

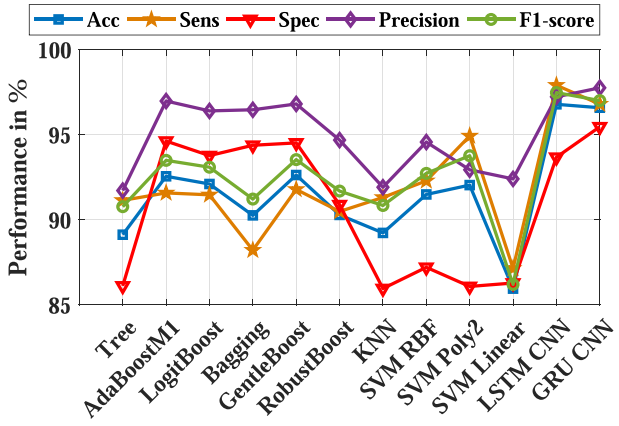

Fig. 7 – The average of performance measures of ML classifiers using WPD and the proposed recurrent CNN methods across 17 patients cross-validation set.

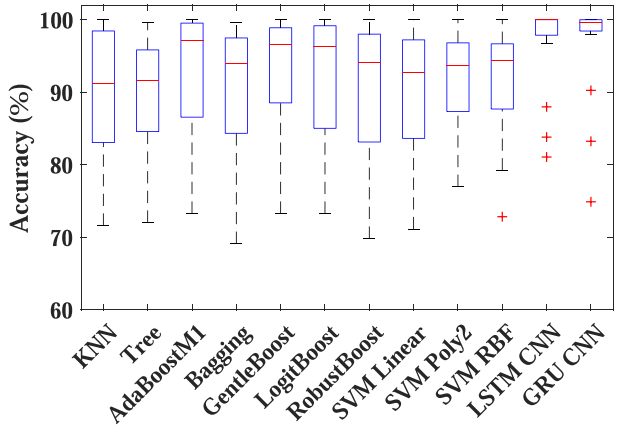

Fig. 8 – Acc performance for ML classifiers using WPD and the proposed recurrent CNN methods across 17 patients cross-validation set (boxes extend from the 25th to the 75th percentile, median in red).

tures in the BG region during the DBS surgery [12,24]. As a result, till now the majority of DBS centers adopt MER for intraoperative refinement of the target localization in addition to optimal trajectory selection [40,17]. In spite of being effective and offers significant neuronavigation [18], MER carries the risk of intracranial hemorrhage [22,23] as well as expanding the surgery time, crucial subjective judgment [24], keeping the patient in awake condition [2] and laborious clinical process that entails high expertise in MER auditory as previously alluded [15]. Indeed, during typical DBS surgery, the neurosurgeon may need to adjust the electrode trajectory 2 or 3 times, which could result further damage to the patient's brain. Therefore, the presented study is tailored towards considering a more robust guidance tool for accurate insertion of the DBS electrode while the patient in an unconscious state.

LFP signals which provide the activity of neuronal populations, instead of single neurons could be more advantageous and robust than MER for optimal target confirmation in PD. Besides, LFP signals are typically sensitive to oscillatory firing patterns and quantitative, while MER is qualitative and open to inter-subject diversity [32]. Also, several researchers indicated that LFP signals show correlation with motor and non-motor symptoms of PD disease [41,42]. Furthermore, Feldmann et al. [43] analyzed incidence and infection characteristics of a group of more than 380 patients who took part in LFP recordings. They demonstrated that LFP is a safe procedure and encourages the evolution of adaptive stimulation protocols. Moreover, to establish the functional role of LFP signals intraoperatively and investigate whether they can contribute to STN localization during DBS surgery, ozturk et al. [29] have performed the first double-blinded pilot study to compare between the clinical outcomes of using either guided MER or LFP for randomly implanting 10 PD patients in both hemispheres of STN. The electrophysiologist relied on visual and auditory inspection of MER signals to provide the final decision about STN localization, while intraoperative signal processing and ML algorithms were employed to give LFP-based decisions. The performance of each modality was gauged three months later by a neurologist. They reported same or higher clinical outcomes when using LFP for targeting. Consequently, DBS surgery based on LFP might possibly lend itself to a significant computerized system for decoding complicated intraoperative neurophysiology as an alternative solution to the current scenario [27]. Accordingly, in the present study, a deep recurrent convolutional neural networks model is developed to automatically assist the decision making in localizing the dorsal and ventral borders of STN in LFP signals. GRU and LSTM were employed individually as the recurrent layer so as to assemble two models. Both layers were used due to their ability to remember either short or long sequences.

Meanwhile, researchers reported that LFP signals can expose pivotal characteristics regarding electrophysiological neural rhythms of STN region [26,28]. In their contribution, authors in [28] presented an implementation of a divisive hierarchical clustering algorithm, capable of differentiating between the functional regions along the electrode trajectory in DBS. They concluded that the features extracted from the neurophysiological LFP signals are legitimate and indicative to detect the boundaries of the STN. Kostoglou et.al [35] employed a number of neurophysiological interpretable fea-

tures with an ensemble of decision trees (i.e. Random Forests) to predict subject-specific DBS response with regards to the associated clinical improvement gauged by unified Parkinson's disease rating scale. In [32], several spectral features were extracted from LFP to predict the optimal track for STN localization. For classification, they employed linear discriminant analysis classifier and obtained highest prediction accuracy of 80%.

It is clear that previous studies concerning LFP signals, have exploited specially-designed techniques to extract, normalize and select engineered features capable of maintaining vital neuronal bio-markers relating to various structures [22,23,26,33]. Then, supervised and unsupervised ML models were employed for training in order to aid the electrode implantation inside the STN during the clinical practice as enumerated earlier [28,35]. Although with their own merits, the reported traditional ML models might be less effective. Such as they are exposed to several immanent shortcomings related to the model training on limited datasets, among others, biasing, design errors and lower performance when validated on a bigger and unknown datasets.

Individual performance of each feature does not simply imply the optimal combinations of features due to important feature interactions. Also, addition of more features does not necessarily contribute to improving the classification accuracy owing to the presence of redundant features. Therefore, exhaustive search is crucial to find the finest combination of features and classifiers [44]. Unlike previous studies, this work is focused on developing a minimalist end-to-end DL model capable of uncovering the optimal feature subsets. This is done without any information reduction by designing feature extraction, normalization and selection in addition to classification protocols. Moreover, to avoid any sort of biasing, Leave CV was used to gauge the classification performance of the proposed methods. This validation technique is used particularly with smaller datasets, similar to ours, wherein distinct patients are used for training and testing, in contrast to n-fold cross validation which combine the data from all the patients in both the training and testing sets. Therefore, Leave CV is applicable to real-time scenarios in which a model must be applied on a patient for whom no training data is at hand.

Meantime, DL techniques have shown to significantly increase the efficiency of classification tasks in comparison with traditional ML techniques due to the advancement in computing power and graphics processing unit. Lately, focus on MER signals classification using DL in an attempt to detect the STN anatomical boundaries has similarly been on the rise [2,30]. However, to the best of our knowledge, this is the first study to explore the ability of DL to extract high level signatures from LFP signals regarding the STN region. Three feature groups namely, Power, HHT and WPD were extracted and fed to 10 ML classifiers in order to confront the performance of the proposed DL models against the existing methods in STN detection. Power and HHT were reported in [28] as informative and able to reveal essential biomarkers from LFP signals about STN. While WPT is established to produce higher frequency resolution than the traditional WT. Therefore, WPT demonstrates further information of low and high frequency components which provide complete representations of the frequency profile of LFPs. In WPT, for five level decomposition, the spectral bandwidth of all sub-bands is 11.875 Hz. These fixed-frequency bandwidth features could improve the performance. The experimental results signify difference between WPT coefficients of LFP signals from STN and Non-STN regions in the beta and gamma frequency sub-bands. These findings are inline with previous studies [22,23,26,32,33].

Despite that the calculation of WPD is considered to be less computationally expensive than HHT and Power, WPD is found to be the most representative feature group to determine the neurophysiological boundaries of STN. Such as, WPD accomplished mean F1-score between 86.21% and 93.77%, while Power yielded mean F1-score between 80.76% and 86.10% and HHT obtained mean F1-score between 76.11% and 87.69% (see Table 3). Although the results indicate that most of these features, especially WPD, demonstrate distinctive differences in STN and Non-STN, no single feature is able to differentiate between the two regions on its own attributed to the overlap between these regions and matching electrophysiological characteristics of structures such as, STN and SNR. The proposed two recurrent CNN models outperformed all the ML classifiers with the three feature groups. LSTM CNN and GRU CNN achieved mean F1-score of 97.48% and 97.01% which is encouraging for automated STN detection (see Table 4). It is evident that the proposed 19-layered DL models are effective to learn the subtle changes regarding STN region from the non-linear and non-stationary LFP signals without any information reduction. Whereas, manual feature extraction and selection steps, which are required in the traditional ML models, are computationally intractable and raise the potential for loss of critical high-frequency components and neural activity characteristics. These results manifest an evidence that LFP can be strategically combined with DL in the operating room for chronic DBS STN localization.

In this work, we are concerned with an alternative intraoperative application of the LFP signals classification instead of the strict real-time application. We believe that an intraoperative decision support system could be accomplished as fast post-exploration classification procedure that the surgical team can exploit after the planned trajectory has been fully investigated, consequently during the revision phase (i.e., At each step, once the exploration is completed, LFP signals can be classified using the proposed DL model as an immediate information for the surgical team to support the clinical decision). Also, the computational load for LSTM CNN and GRU CNN is well suited to real-time implementation, being nearly 200 ms for each patient. In fact, the proposed methods are executed in MATLAB software, which is a portable program and can be installed in any clinic or hospital as a trusted tool, helping the surgical team to automate the localization of STN during DBS surgery. In addition, 1s LFP recordings are used as the input to the proposed DL model and, therefore, the surgical team do not need to wait for a long time at each step to determine whether the electrode in STN or Non-STN region.

Reducing the necessary listening time at each position along the electrode trajectory is crucial to improve the patient comfort. Authors in [45,46,15] reported that 1s signals are enough to attain discriminating features and obtain accurate

predictions. Besides, short LFP samples are beneficial to speed-up the batch normalization step in the LFE part and decrease the number of parameters that have to be learned in the first dense layer. In view of this, as a trade-off between the computing efficiency and capacity, 1s long recordings were chosen as the length. Since LFP data homogeneity is affected by inter-subject diversity in neurophysiology as well as recording characteristics variability which would induce high variation in amplitude of LFP signals from all the patients and generate unstable dataset, the first preprocessing technique is to assign the data to a certain range of values and remove the outliers. As a result, we conclude that the input LFP data normalization is essential for subsequent analysis and convenience of DL training. The main limitation of this study is the demand for larger dataset in order to fabricate a trustworthy STN detection system such as data insufficiency is important for learnability of DL models. Nevertheless the proposed methods showed good performance, in line with previous studies, on a small dataset from only 17 PD patients, investigating an offline yet still intraoperative LFP signals based classification.

5. Conclusion

In this work, we have developed two recurrent CNN models for LFP analysis to identify the neurophysiological borders of STN, allowing for less subjective interpretation by reducing the necessary time required for recording electrophysiological signals at each position along the electrode trajectory. Importantly, this work shows that integrating recurrent layers into CNN produces an efficient model which can considerably categorize the relevant morphological features of LFP signals and reveal the hidden non-linear signatures about STN region. The designed recurrent CNN models benefit from the advantages of CNN in terms of local feature extraction without information reduction, and from the advantages of recurrent layers in terms of managing individual features by defining the characteristics of the global vectors. The experimental results showed that the proposed models outperformed the state-of-the-art methods (i.e Power, HHT and WPD) in the field of LFP analysis. As LSTM CNN yielded an average Acc of 96.79%, Sens of 97.91%, Spec of 93.68%, precision of 97.23% and F1-score of 97.48%, while GRU CNN achieved an average Acc of 96.59%, Sens of 96.80%, Spec of 95.47%, precision of 97.76% and F1-score of 97.01%. Therefore, the proposed system can accurately localize the STN region with 1s LFP signal. Given the lower computational cost of LFP and the robustness of the proposed approaches, DBS centers can consider LFP as a promising path for intraoperative integration of a strategic feedback modality into the surgical decision support system for chronic electrode implantation. Besides, an automated investigation of LFP signals with our recurrent CNN model could thus greatly ameliorate the patient comfort and improve the DBS procedure via significantly reducing the surgery time.

For future work, we plan to investigate on the efficiency of the recurrent CNN models by gauging their performance on another LFP datasets recorded by different hardware from other institutions. Finally, we would further extend the DL model with other optimization and ML algorithms. Currently, we are employing fully-connected neuron and SoftMax layers for classification. We hypothesize that replacing them with a ML classifier to take advantage of its learnability and exploiting technique such as genetic algorithm for optimization of features and parameters could enhance the classification efficacy.

CRediT authorship contribution statement

Mohamed Hosny: Methodology, Software, Visualization, Validation, Writing- Original draft preparation, Writing- Reviewing and Editing. **Minwei Zhu:** Resources, Data curation. **Yixian Su:** Writing- Reviewing and Editing. **Wenpeng Gao:** Conceptualization, Project administration, funding acquisition, Writing- Reviewing and Editing. **Yili Fu:** Supervision.

Declaration of Competing Interest

The authors declare that they have no known competing financial interests or personal relationships that could have appeared to influence the work reported in this paper.

Acknowledgement

Funding: This work was supported by the National Natural Science Foundation of China (Grant No.81201150). It was also supported by Natural Science Foundation of Heilongjiang Province of China (Grant No. LH2019F021).

Statements of ethical approval: For this review article, the authors did not undertake work that involved human participants or animals.

REFERENCES

[1] Xiao Y, Lau JC, Hemachandra D, Gilmore G, Khan AR, Peters TM. Image Guidance in Deep Brain Stimulation Surgery to Treat Parkinson's Disease: A Comprehensive Review. IEEE Trans Biomed Eng 2021;68(3):1024–33.

[2] Martin T, Peralta M, Gilmore G, Sauleau P, Haegelen C, Jannin P, et al. Extending convolutional neural networks for localizing the subthalamic nucleus from micro-electrode recordings in Parkinson's disease. Biomed Signal Process Control September 2020;2021(67) 102529.

[3] Valsky D, Blackwell KT, Tamir I, Eitan R, Bergman H, Israel Z. Real-time machine learning classification of pallidal borders during deep brain stimulation surgery. J Neural Eng 2020;17 (1).

[4] Zhang Y, Xu S, Xiao G, Song Y, Gao F, Wang M, et al. High frequency stimulation of subthalamic nucleus synchronously modulates primary motor cortex and caudate putamen based on dopamine concentration and electrophysiology activities using microelectrode arrays in Parkinson's disease rats. Sensors Actuators B: Chem 2019;301 (June) 127126.

[5] Velisar A, Syrkin-Nikolau J, Blumenfeld Z, Trager M, Afzal M, Prabhakar V, et al. Dual threshold neural closed loop deep brain stimulation in Parkinson disease patients. Brain Stimul 2019;12(4):868–76.

[6] Alper MA, Goudreau J, Daniel M. Pose and optical flow fusion (poff) for accurate tremor detection and quantification. Biocybernetics Biomed Eng 2020;40(1):468–81.
[7] Chen KHS, Chen R. Invasive and Noninvasive Brain Stimulation in Parkinson's Disease: Clinical Effects and Future Perspectives. Clin Pharmacol Ther 2019;106(4):763–75.
[8] Boller JK, Barbe MT, Pauls KAM, Reck C, Brand M, Maier F, et al. Decision-making under risk is improved by both dopaminergic medication and subthalamic stimulation in Parkinson's disease. Exp Neurol 2014;254:70–7.
[9] Barbe MT, Tonder L, Krack P, Debû B, Schüpbach M, Paschen S, et al. Deep Brain Stimulation for Freezing of Gait in Parkinson's Disease With Early Motor Complications. Movement Disorders 2020;35(1):82–90.
[10] Khawaldeh S, Tinkhauser G, Shah SA, Peterman K, Debove I, Nguyen TAK, et al. Subthalamic nucleus activity dynamics and limb movement prediction in Parkinson's disease. Brain: J Neurol 2020;143(2):582–96.
[11] Mao Z, Ling Z, Pan L, Xu X, Cui Z, Liang S, et al. Comparison of Efficacy of Deep Brain Stimulation of Different Targets in Parkinson's Disease: A Network Meta-Analysis. Frontiers in Aging Neuroscience 2019;11(FEB):1–8. .
[12] Rui K, Maszczyk T, An A, See Q, Dauwels J, Kon N, et al. A review on microelectrode recording selection of features for machine learning in deep brain stimulation surgery for Parkinson ' s disease. Clin Neurophysiol 2019;130(1):145–54.
[13] Farrokhi F, Buchlak QD, Sikora M, Esmaili N, Marsans M, McLeod P, et al. Investigating Risk Factors and Predicting Complications in Deep Brain Stimulation Surgery with Machine Learning Algorithms. World Neurosurgery 2020;134:468–81.
[14] Rolston JD, Englot DJ, Starr PA, Larson PS. An unexpectedly high rate of revisions and removals in deep brain stimulation surgery: analysis of multiple databases. Parkinsonism Related Disorders 2016;33:72–7.
[15] Peralta M, Bui QA, Ackaouy A, Martin T, Gilmore G, Haegelen C, et al. SepaConvNet for Localizing the Subthalamic Nucleus Using One Second Micro-electrode Recordings. Proceedings of the Annual International Conference of the IEEE Engineering in Medicine and Biology Society, EMBS 2020;2020-July:888–893. .
[16] Lozano CS, Ranjan M, Boutet A, Xu DS, Kucharczyk W, Fasano A, et al. Imaging alone versus microelectrode recording-guided targeting of the STN in patients with Parkinson's disease. J Neurosurg 2019;1306(6):1847–52.
[17] Mehanna R, Machado AG, Connett JE, Alsaloum F, Cooper SE. Intraoperative Microstimulation Predicts Outcome of Postoperative Macrostimulation in Subthalamic Nucleus Deep Brain Stimulation for Parkinson's Disease. Neuromodulation 2017;20(5):456–63.
[18] Hartmann CJ, Fliegen S, Groiss SJ, Wojtecki L, Schnitzler A. An update on best practice of deep brain stimulation in parkinson's disease. Therapeutic Adv Neurol Disorders 2019;12:1–20.
[19] Liu X, Zhang J, Fu K, Gong R, Chen J, Zhang J. Microelectrode Recording-Guided Versus Intraoperative Magnetic Resonance Imaging-Guided Subthalamic Nucleus Deep Brain Stimulation Surgery for Parkinson Disease: A 1-Year Follow-Up Study. World Neurosurgery 2017;107:900–5.
[20] Lee PS, Weiner GM, Corson D, Kappel J, Chang YF, Suski VR, et al. Outcomes of interventional-MRI versus microelectrode recording-guided subthalamic deep brain stimulation. Frontiers in Neurology 2018;9(APR):1–8. .
[21] Hosny M, Zhu M, Gao W, Fu Y. A novel deep LSTM network for artifacts detection in microelectrode recordings. Biocybern Biomed Eng 2020;40(3):1052–63.
[22] Telkes I, Ince NF, Onaran I, Abosch A. Localization of subthalamic nucleus borders using macroelectrode local field potential recordings. In: 2014 36th Annual International Conference of the IEEE Engineering in Medicine and Biology Society, EMBC. p. 2621–4.
[23] Telkes I, Ince NF, Onaran I, Abosch A. Spatio-spectral characterization of local field potentials in the subthalamic nucleus via multitrack microelectrode recordings. Proceedings of the Annual International Conference of the IEEE Engineering in Medicine and Biology Society, EMBS 2015:5561–5564. .
[24] Karthick PA, Wan KR, An Qi AS, Dauwels J, King NKK. Automated detection of subthalamic nucleus in deep brain stimulation surgery for parkinson's disease using microelectrode recordings and wavelet packet features. J Neurosci Methods 2020;343:108826.
[25] Valsky D, Marmor-Levin O, Deffains M, Eitan R, Blackwell KT, Bergman H, et al. Stop! border ahead: Automatic detection of subthalamic exit during deep brain stimulation surgery. Mov Disord 2017;32(1):70–9.
[26] Telkes I, Sabourin S, Durphy J, Adam O, Sukul V, Raviv N, et al. Functional Use of Directional Local Field Potentials in the Subthalamic Nucleus Deep Brain Stimulation. Front Human Neurosci 2020;14(April):1–9.
[27] Telkes I, Viswanathan A, Jimenez-Shahed J, Abosch A, Ozturk M, Gupte A, et al. Local field potentials of subthalamic nucleus contain electrophysiological footprints of motor subtypes of Parkinson's disease. Proc National Acad Sci USA 2018;115(36):E8567–76.
[28] Cao L, Jie L, Zhou Y, Liu Y, Liu H. Automatic feature group combination selection method based on GA for the functional regions clustering in DBS. Comput Methods Programs Biomed 2020;183.
[29] Ozturk M, Telkes I, Jimenez-Shahed J, Viswanathan A, Tarakad A, Kumar S, et al. Randomized, Double-Blind Assessment of LFP Versus SUA Guidance in STN-DBS Lead Implantation: A Pilot Study. Front Neurosci 2020;14 (June):1–12.
[30] Khosravi M, Atashzar SF, Gilmore G, Jog MS, Patel RV. Intraoperative Localization of STN during DBS Surgery using a Data-driven Model. IEEE J Transl Eng Health Med 2020;8:1–9.
[31] Hosny M, Zhu M, Gao W, Fu Y. Detection of subthalamic nucleus using novel higher-order spectra features in microelectrode recordings signals. Biocybern Biomed Eng 2021;41(2):704–16.
[32] Telkes I, Jimenez-Shahed J, Viswanathan A, Abosch A, Ince NF. Prediction of STN-DBS electrode implantation track in Parkinson's disease by using local field potentials. Front Neurosci 2016;10(MAY):1–16.
[33] Cao L, Li J, Zhou Y, Liu Y, Zhao Y, Liu H. Online identification of functional regions in deep brain stimulation based on an unsupervised random forest with feature selection. J Neural Eng 2019;16(6).
[34] Cagnan H, Dolan K, He X, Contarino MF, Schuurman R, Van Den Munckhof P, et al. Automatic subthalamic nucleus detection from microelectrode recordings based on noise level and neuronal activity. Journal of Neural Engineering 2011;8(4):046006 (9 pages). .
[35] Kostoglou K, Michmizos KP, Stathis P, Sakas D, Nikita KS, Mitsis GD. Classification and Prediction of Clinical Improvement in Deep Brain Stimulation from Intraoperative Microelectrode Recordings. IEEE Trans Biomed Eng 2017;64 (5):1123–30.
[36] Pinzon-Morales RD, Garces-Arboleda M, Orozco-Gutierrez AA. Automatic identification of various nuclei in the basal ganglia for Parkinson's disease neurosurgery. Proceedings of the 31st Annual International Conference of the IEEE Engineering in Medicine and Biology Society: Engineering the Future of Biomedicine, EMBC 2009 2009:3473–3476.

[37] Hammad M, Iliyasu AM, Subasi A, Ho ESL, El-Latif AAA. A Multitier Deep Learning Model for Arrhythmia Detection. IEEE Trans Instrum Meas 2021;70:1–9.
[38] Shamir RR, Duchin Y, Kim J, Patriat R, Marmor O, Bergman H, et al. Microelectrode Recordings Validate the Clinical Visualization of Subthalamic-Nucleus Based on 7T Magnetic Resonance Imaging and Machine Learning for Deep Brain Stimulation Surgery. Clin Neurosurg 2019;84(3):749–56.
[39] Schlaier JR, Habermeyer C, Janzen A, Fellner C, Hochreiter A, Proescholdt M, et al. The influence of intraoperative microelectrode recordings and clinical testing on the location of final stimulation sites in deep brain stimulation for Parkinson's disease. Acta Neurochir 2013;155(2):357–66.
[40] Kocabicak E, Alptekin O, Aygun D, Yildiz O, Temel Y. Microelectrode recording for deep brain stimulation on the subthalamic nucleus in patients with advanced parkinson's diesease: advantage or loss of time. Turk Neurosurg 2019;29 (5):677–82.
[41] Thompson JA, Lanctin D, Ince NF, Abosch A. Clinical implications of local field potentials for understanding and treating movement disorders. Stereotact Funct Neurosurg 2014;92(4):251–63.
[42] Priori A, Foffani G, Rossi L, Marceglia S. Adaptive deep brain stimulation (aDBS) controlled by local field potential oscillations. Exp Neurol 2013;245:77–86.
[43] Feldmann LK, Neumann Wj, Faust K, Schneider GH, Kühn AA. Risk of Infection after Deep Brain Stimulation Surgery with Externalization and Local-Field Potential Recordings: Twelve-Year Experience from a Single Institution. Stereotactic and Functional Neurosurgery 2021;:1–9. .
[44] Rajpurohit V, Danish SF, Hargreaves EL, Wong S. Optimizing computational feature sets for subthalamic nucleus localization in DBS surgery with feature selection. Clin Neurophysiol 2015;126(5):975–82.
[45] Schiaffino L, Rosado Munoz A, Guerrero Martinez J, Francés Villora J, Gutiérrez A, Martinez Torres I, et al. STN area detection using K-NN classifiers for MER recordings in Parkinson patients during neurostimulator implant surgery. J Phys: Conf Ser 2016;705(1):441–4.
[46] Vargas Cardona HD, Álvarez MA, Orozco ÁA. Multi-task learning for subthalamic nucleus identification in deep brain stimulation. Int J Mach Learn Cybern 2018;9(7):1181–92.